2016

Influence of Nb on the β → α" martensitic phase transformation and properties of the newly designed Ti-Fe-Nb alloys

Shima Ehtemam-Haghighi
Edith Cowan University

Yujing Liu
Edith Cowan University

Guanghui Cao

Lai-Chang Zhang
Edith Cowan University

10.1016/j.msec.2015.11.072
This is an Author's Accepted Manuscript of:
Ehtemam-Haghighi, S., Liu, Y., Cao, G., & Zhang, L. C. (2016). Influence of Nb on the β→ α "martensitic phase transformation and properties of the newly designed Ti–Fe–Nb alloys. Materials Science and Engineering: C, 60, 503-510.
https://doi.org/10.1016/j.msec.2015.11.072

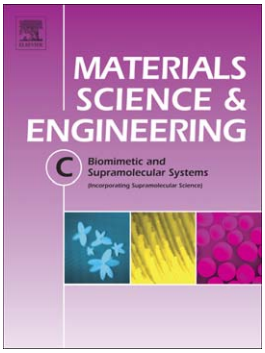

Influence of Nb on the $\beta \rightarrow \alpha$" martensitic phase transformation and properties of the newly designed Ti-Fe-Nb alloys

Shima Ehtemam-Haghighi, Yujing Liu, Guanghui Cao, Lai-Chang Zhang

PII: S0928-4931(15)30603-2
DOI: doi: 10.1016/j.msec.2015.11.072
Reference: MSC 5985

To appear in: *Materials Science & Engineering C*

Received date: 13 July 2015
Revised date: 6 November 2015
Accepted date: 30 November 2015

Please cite this article as: Shima Ehtemam-Haghighi, Yujing Liu, Guanghui Cao, Lai-Chang Zhang, Influence of Nb on the $\beta \rightarrow \alpha$" martensitic phase transformation and properties of the newly designed Ti-Fe-Nb alloys, *Materials Science & Engineering C* (2015), doi: 10.1016/j.msec.2015.11.072

Influence of Nb on the β→α'' martensitic phase transformation and properties of the newly designed Ti-Fe-Nb alloys

Shima Ehtemam-Haghighi[1*], Yujing Liu[1], Guanghui Cao[2], Lai-Chang Zhang[1*]

[1]*School of Engineering, Edith Cowan University, 270 Joondalup Drive, Joondalup, Perth, WA 6027, Australia*

[2]*Department of Materials Engineering, Shanghai Key Laboratory of Modern Metallurgy and Materials Processing, Shanghai University, 149 Yanchang Road, Shanghai 200072, China*

Abstract

A series of Ti-7Fe-xNb (x = 0, 1, 4, 6, 9, 11 wt%) alloys was designed and cast to investigate the β→α'' martensitic phase transformation, β phase stability, the resulting microstructure and mechanical properties. Phase analysis revealed that only Ti-7Fe-11Nb alloy shows a single body-centered cubic β phase microstructure while the others are comprised of β and orthorhombic α'' phases. Moreover, Nb addition up to 11wt% enhances the stability and volume fraction of β phase in the microstructure, hence reducing the propensity of the alloy system to form α'' phase during quenching. Compressive yield strength and hardness of the alloys are (985-1847) MPa and (325-520) Hv respectively. Additionally, Ti-7Fe-11Nb possesses the lowest Young's modulus (84 GPa) and the highest deformability (42% strain) amongst the designed alloys due to the single β phase microstructure. This high deformability is also corroborated by the large plastic deformation zone underneath the Vickers indenter. In contrast, the fractured surfaces of Ti-7Fe and Ti-7Fe-1Nb alloys after compressive tests mostly contain shallow dimples, verifying their low ductility. The good combination of mechanical properties obtained for Ti-7Fe-11Nb renders it more desirable than commonly used CP-Ti and Ti-6Al-4V materials and makes it a promising candidate for biomedical application.

Keywords: Titanium alloy; Phase stability; Microstructure; Mechanical property; Shear bands

* Corresponding author. Tel.: +61863042322.
E-mail addresses: sehtemam@our.ecu.edu.au, sehtemam@gmail.com (Shima Ehtemam-Haghighi), l.zhang@ecu.edu.au, lczhangimr@gmail.com (Lai-Chang Zhang).

1. Introduction

Titanium and titanium alloys have been extensively used for manufacturing load-bearing orthopaedic implants [1, 2] due to their combination of unique properties including low density, high specific strength, superior corrosion resistance, excellent biocompatibility and low modulus of elasticity [3, 4]. Early in the development of materials for orthopaedic applications, CP-Ti was used as an implant material but later it was substituted by Ti-6Al-4V due to its higher strength and improved corrosion resistance compared to CP-Ti [5, 6]. While Ti-6Al-4V has been one of the most widely used titanium alloys for medical implants, it has been reported that the release of toxic aluminium (Al) and vanadium (V) ions may induce some long-term serious health problems [6]. Consequently, Al-free and V-free titanium alloys have been developed [7, 8]. However, in terms of mechanical properties these developed alloys are relatively similar to Ti-6Al-4V as they belong to α or (α+β)-type titanium alloys. Their modulus of elasticity values are still considerably higher than that of bone [7] which can lead to the stress-shielding phenomenon [3]. This phenomenon, which decreases the load stimulus for continued bone remodelling, reduces the bone density and consequently leads to loosening of the implant and subsequent refracture of the bone [3, 8].

Because of their body-centered cubic (bcc) crystalline structure, the β-type titanium alloys exhibit an elastic modulus lower than α and (α+β)-type alloys, which may mitigate the stress shielding phenomenon [9], hence promoting bone remodelling [10, 11]. It is widely known that certain phases/crystal structures of titanium alloys may be stabilized through incorporation of specific alloying elements [5, 6]. It is known that α-stabiliser elements include Al, O, N and Sn, whereas β-stabilizers are Fe, Nb, Mo and Ta [5]. In the last two decades, research on titanium alloys for biomedical applications has increasingly focused on developing β-type Ti alloys containing non-toxic β-stabilizer alloying elements like Nb, Ta, Zr, Mo, for example, Ti–12Mo–6Zr–2Fe [3], Ti–35.3Nb–5.1Ta–7.1Zr [3] and Ti-24Nb-4Zr-8Sn [12]. Such alloys have better properties than α and (α+β)-type titanium alloys, including good ductility and high strength in combination with lower modulus of elasticity [8, 13]. However, most of these developed β-type titanium alloys contain a

great amount of expensive elements with high density and melting points such as Ta, Nb, Zr and Mo. Additionally, as these elements are rare in the earth's crust, the recently developed alloys containing a high value of these expensive elements could not compete with the commercial alloys [8]. Consequently, researchers have now focused on designing new β-type titanium alloys which include non-toxic, low-cost, abundant metals such as Fe, Mn and Cr to reduce consumption of high cost elements like Ta, Nb, Zr and Mo [3, 8]. Example of these alloys include Ti–Mn–Fe [3], Ti–Cr–Sn–Zr [3] and Ti–Fe–Ta–Zr [14].

While Fe is an attractive low cost β-stabilizer element along with the β-stabilizer and biocompatible component, Nb, for developing β-type titanium alloys [6], few studies have addressed the relevant properties of Ti-Fe based alloys. Researchers have shown that the stability of β phase and mechanical properties of β-type Ti alloys are strongly affected by the existence of martensitic phases, like α", α' and ω, which may precipitate in metastable β-type Ti alloys upon quenching to room temperature or deformation [15]. Therefore, it is important to investigate the effect of β-stabilizer content on the stability of β phase and properties of β-type Ti alloys. As such, the present study focuses on a series of designed Ti-Fe-Nb alloys in which the influence of Nb content on β→α" martensitic phase transformation and particularly on the stability of β phase during casting is investigated. It also assesses the effects of Nb content on the microstructural and mechanical characteristics of the Ti-Fe-Nb alloys.

2. Experimental

Ti-7Fe-xNb (x = 0, 1, 4, 6, 9, 11 wt%) alloys were designed and fabricated from 99.9% pure raw Ti, Fe and Nb metals using cold crucible levitation melting (CCLM) under an argon atmosphere. The CCLM furnace, a type of induction melting furnace, was composed of a water-cooled crucible made from high purity copper segments. Induction coils were wrapped around the crucible and connected to a frequency inverter power supply. After complete melting of the raw metals and subsequent mixing, the electric power was turned off and the molten metals were solidified into an ingot in the water-cooled copper crucible. The alloy ingots were flipped and re-

melted four times to promote their chemical homogeneity. The as-cast alloy ingots (hereafter referred to as the "as-cast" samples) were 8 mm in diameter and 100 mm long. The as-cast samples were sectioned using a Buehler Isomet low speed diamond saw to obtain specimens for various purposes. The phase constitution in the alloys was identified by X-Ray diffraction (XRD) using PANalytical EMPYREAN diffractometer with Cu Kα radiation (λ = 1.5406 nm). XRD patterns were recorded at a step size of 0.01° and scanning speed of 1 deg/min. The integrated areas for α″ and β diffraction peaks in the XRD spectra were determined by using the peak-fitting program, Fityk, with Pearson VII function [16, 17]. Based on the integrated areas, the volume fraction (V_f) of α″ and β phases were calculated in a similar manner to Ref. [18] using the equations below:

$$V_{f_{(\alpha'')}} = \frac{A_{\alpha''}}{A_{\alpha''} + A_{\beta}} \quad (1)$$

$$V_{f_{(\beta)}} = \frac{A_{\beta}}{A_{\alpha''} + A_{\beta}} \quad (2)$$

where $V_{f_{(\alpha'')}}$ and $V_{f_{(\beta)}}$ are the volume fractions and $A_{\alpha''}$ and A_{β} are the total integrated areas, corresponding to α″ and β phases, respectively.

To characterize microstructural features, samples surfaces were prepared using conventional grinding and polishing procedures followed by etching in Kroll's solution (5 vol% HF, 30 vol% HNO_3 and 65 vol% H_2O). The microstructures of the alloys were examined using a Zeiss optical microscope (OM) and elemental mapping was conducted by scanning electron microscopy (SEM, Jeol JSM 6000) with an energy dispersive X-ray detector (EDX). To evaluate the mechanical properties of the as-cast titanium alloys, compressive and hardness tests were conducted. To determine the compressive yield stress, plastic strain and modulus of elasticity, a compressive test was carried out on the cylindrical specimens of 8 mm in diameter and 16 mm long using an Instron 5980 universal testing machine at a crosshead speed of 0.001 mm/s at room temperature. To ensure the accuracy of Young's modulus, a clip-on extensometer attached to the specimen was used to measure the strain. Young's modulus was determined for each specimen as the slope of the linear portion of stress-strain curve [19]. For each alloy composition, the average value of

Young's modulus was calculated from 5 repeat tests. In addition, the fractured surface of any specimen which broke during compressive testing was observed using SEM.

Vickers hardness measurements of the polished samples were carried out using a ZwickRoell hardness testing machine with a load of 5 kgf and a dwell time of 30 s. The average hardness values were obtained from at least 10 measurements. To characterize the deformed morphology beneath the Vickers indentation, the bonded interface technique was employed [20, 21]. Thereafter, the deformation morphology beneath the indentation imprint was examined by SEM.

3. Results and discussion

3.1. Phase analysis and microstructure

Fig. 1 shows the XRD profiles of Ti-7Fe and the ternary Ti-7Fe-xNb alloys, which indicate that all alloys except Ti-7Fe-11Nb are comprised of bcc β and orthorhombic α" phases. Additionally, the TiFe intermetallic compound is not presented in all alloys because of the low Fe content in the studied alloys [22]. Based on the XRD patterns, the volume fractions of the alloy phases were estimated; according to Table 1, Ti-7Fe contains the lowest β volume fraction (V_f = 62%) and the highest volume fraction of α" phase (V_f = 38%). This athermal α" orthorhombic structure, induced by fast cooling, was attained from a distorted hexagonal unit cell in which the *c*-axis of the orthorhombic unit cell correlates with *c*-axis of the hexagonal unit cell whereas *a* and *b* correspond to the orthogonal axis of the hexagonal unit cell [22]. The α" orthorhombic martensite, which can be formed upon quenching without assistance from external stress, has also been recognised in other Ti alloy systems [5, 23].

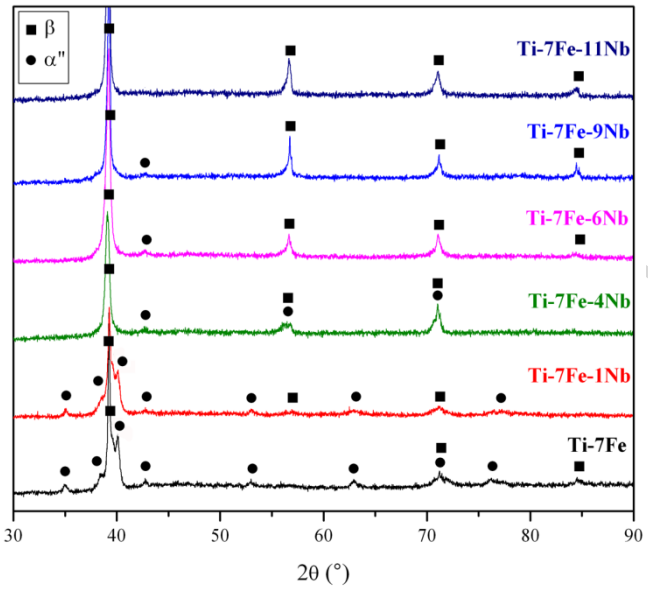

Fig. 1 XRD patterns of the as-cast Ti–7Fe–xNb alloys.

As presented in Fig. 1, when 1 wt% Nb is introduced into the Ti-7Fe alloy, the intensity of the peaks corresponding to α" phase decreases, hence the volume fraction of this phase (V_f = 34%) reduces. With addition of 4 or 6 wt% Nb to Ti-7Fe alloy, the number of the α" phase peaks (i.e. around 53°, 63° and 76°) decreases suggesting that the formation of α" phase is greatly suppressed whereas the intensity of β phase peaks and concentration of β phase increase (Table 1). When Nb content is 9 wt%, the alloy exhibits the weakest peak of α" phase, while β phase peaks become sharper, hence a significant amount of β phase with bcc crystal structure is retained (Table 1). Finally, the addition of 11 wt% Nb to Ti-7Fe leads to the retention of only β phase as verified by its XRD pattern.

Table 1. Volume fraction (V_f) of α" and β phases in as-cast Ti–7Fe–xNb alloys.

Alloy nominal composition (wt%)	**α" phase V_f (%)**	**β phase V_f (%)**
$Ti_{93}Fe_7$	38	62
$Ti_{92}Fe_7Nb_1$	34	66
$Ti_{89}Fe_7Nb_4$	18	82
$Ti_{87}Fe_7Nb_6$	10	90
$Ti_{84}Fe_7Nb_9$	4	96
$Ti_{82}Fe_7Nb_{11}$	–	100

The stability of β phase is determined by its ability to undergo martensitic transformation (β→α", β→α', β→ω) upon quenching to room temperature or upon deformation [15]. Transition metallic elements such as Nb, Ta, V, Mo, and Cr have long served as β-stabilising elements and are mostly used for producing metastable or stable β-type titanium alloys [15]. In this study, as the Nb concentration of the alloys increases, the stability of β-phase improves whereas the propensity of the Ti-7Fe-xNb system to form α" martensite upon quenching declines. In other words, as more β-stabilizer Nb is added, the β→α" martensitic start temperature [24], M_s, decreases and accordingly the proportion of α" martensite phase in the alloys cooled to room temperature declines.

The stability of β phase can be predicted based on the DV-Xα cluster method [25] and the molybdenum equivalency (Mo_{eq}) parameter [26]. In the DV-Xα cluster method two parameters were defined for calculation [25]. One is the bond order (Bo), which is related to the strength of the covalent bond between Ti and an alloying element. The other is the metal *d*-orbital energy level (Md), which is correlated with the electronegativity and the metallic radius of the alloying elements [14]. For an alloy, the average values of bond order ($\overline{Bo}$) and *d*-orbital energy levels ($\overline{Md}$) are calculated as follows [25, 27]:

$$\overline{Bo} = \sum X_i \cdot (Bo)_i \quad (3)$$

$$\overline{Md} = \sum X_i \cdot (Md)_i \quad (4)$$

where X_i is the atomic fraction of element i in the alloy, $(Bo)_i$ and $(Md)_i$ are the bond order and metal *d*-orbital energy level values for element i, respectively [27].

Additionally, the Mo_{eq} of an alloy can be expressed by the following formula [28]:

$$[Mo]_{eq} = [Mo] + \frac{[Ta]}{5} + \frac{[Nb]}{3.6} + \frac{[W]}{2.5} + \frac{[V]}{1.5} + 1.25[Cr] + 1.25[Ni] + 1.7[Mn] + 1.7[Co] + 2.5[Fe] \quad (5)$$

where $[x]$ indicates the concentration of element x in weight percent [28].

The stability of β phase improves by increasing Bo or decreasing Md and by increasing Mo_{eq} [15, 26]. Table 2 summarizes the calculated values of Mo_{eq}, $\overline{Bo}$ and $\overline{Md}$ of the designed alloys. As indicated, the values for Mo_{eq} are higher than 10 wt% thus classifying all of the alloys into the metastable β category [29]. It is noted that metastable β alloys could also display martensitic

phases in the microstructure during rapid cooling [30]. In this work, Ti-7Fe alloy with the lowest Mo_{eq} value, exhibits the least β phase stability among the metastable β Ti-7Fe-xNb alloys. According to Table 2, with an increase in Nb content of the alloys, the values of Mo_{eq} and $\overline{Bo}$ increase, but $\overline{Md}$ decreases, indicating the enhancement in the β phase stability of the metastable alloys against martensitic (β→α") transformation [31]. The stability of β phase reaches the maximum in Ti-7Fe-11Nb alloy and no α" martensite is formed. This is also evidenced in Fig. 1 and Fig. 2(f).

Table 2. β phase stabilizer indicators for as-cast Ti–7Fe–xNb alloys.

Alloy nominal composition (wt%)	**β stability indicators**		
	$\overline{Bo}$	$\overline{Md}$	Mo_{eq}
$Ti_{93}Fe_7$	2.781	2.357	17.500
$Ti_{92}Fe_7Nb_1$	2.783	2.356	17.777
$Ti_{89}Fe_7Nb_4$	2.787	2.355	18.611
$Ti_{87}Fe_7Nb_6$	2.791	2.353	19.166
$Ti_{84}Fe_7Nb_9$	2.796	2.352	20.000
$Ti_{82}Fe_7Nb_{11}$	2.800	2.350	20.556

The optical microstructures of the Ti-7Fe and Ti-7Fe-xNb alloys after etching are shown in Fig. 2. All alloys, except Ti-7Fe-11Nb, have a two-phase morphology comprising β and α" martensite phases. Ti-7Fe alloy (Fig. 2(a)) exhibits the coexistence of β phase grains and a dense α" martensite phase precipitated in the β matrix.

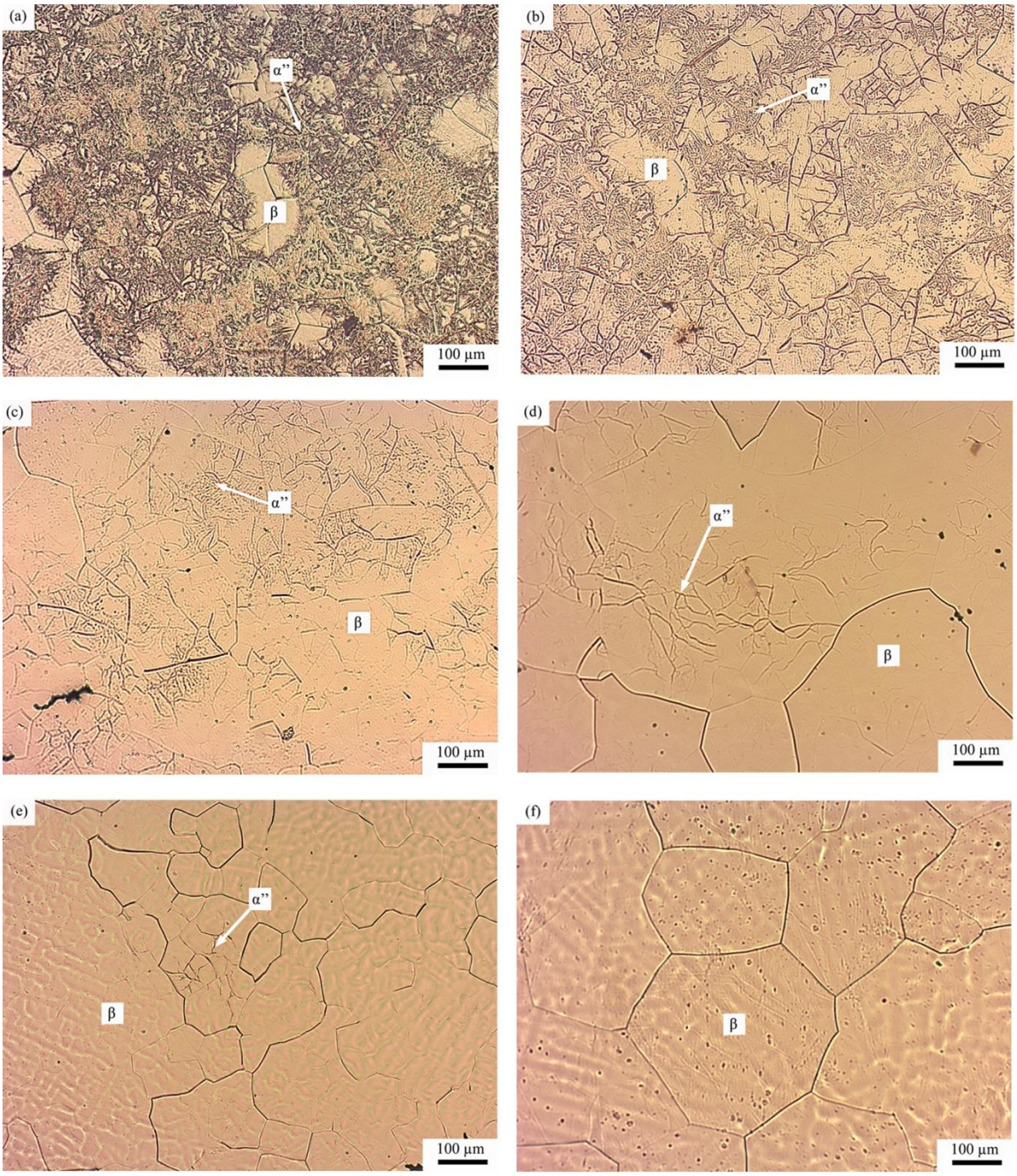

Fig. 2 Optical micrographs of Ti–7Fe–xNb alloys: (a) Ti–7Fe, (b) Ti–7Fe–1Nb, (c) Ti–7Fe–4Nb, (d) Ti–7Fe–6Nb, (e) Ti–7Fe–9Nb, and (f) Ti–7Fe–11Nb.

When 1 or 4 wt% β-stabilizer Nb is added, the quantity of α" phase is decreased (Figs. 2(b) and (c)). Similarly, introducing 6 or 9 wt % Nb to the Ti-7Fe alloy leads to the significant reduction in the amount of α" martensite phase, hence β phase becomes more dominant (Figs. 2(d) and (e)). As can be observed in Fig. 2(f), further addition of Nb to 11 wt% enhances β phase stability so that

the microstructure overwhelmingly contains only β phase. The complete retention of β phase by adding 11 wt% Nb is also proved in the X-ray spectra in Fig. 1. Therefore, based on these results, a higher concentration of Nb increases the stability of β phase and decreases the possibility of α" martensite formation in these metastable β alloys during rapid cooling. The existence of α" martensite phase in the microstructure has also been recognised in other studies which verify the martensitic transformation of β to α" phase [32, 33].

The dendritic substructure in the β grains of the as-cast Ti-7Fe-xNb alloys containing the two highest concentrations of Nb can be seen in Figs. 2 (e) and (f). Fig. 3 displays the back scattered electron (BSE) image and associated Ti, Nb and Fe distribution EDX maps obtained for Ti-7Fe-11Nb alloy. The contrast in the BSE image (Fig. 3(a)) indicates that the dendritic structure in Fig. 2(f) and similarly in Fig. 2(e) is related to chemical segregation during the solidification process of these specified alloys.

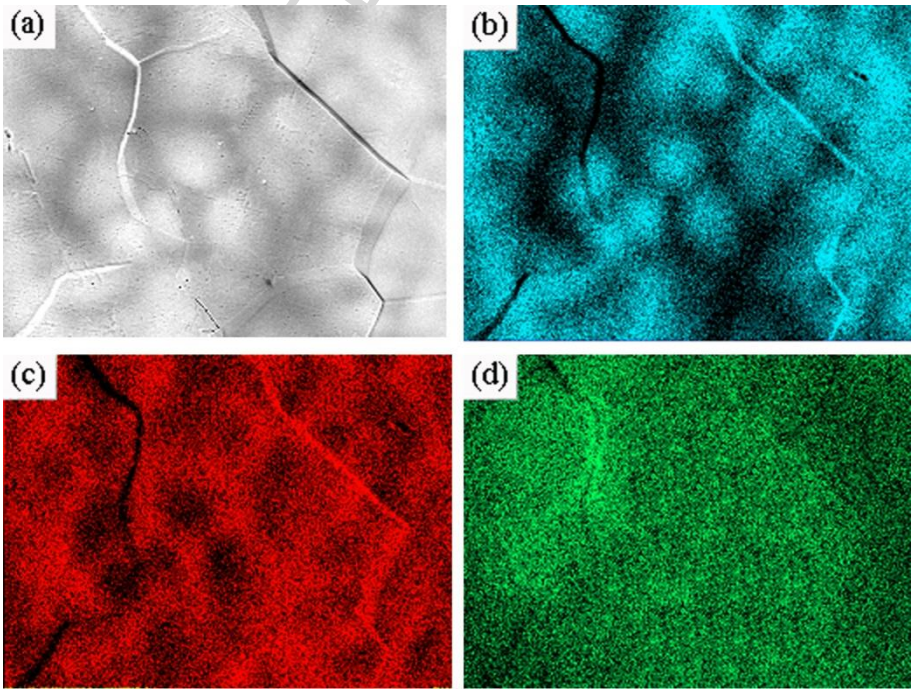

Fig. 3 (a) Backscattered SEM image of Ti–7Fe–11Nb alloy and its X–ray element distribution maps: (b) Nb distribution, (c) Ti distribution and (d) Fe distribution.

The distribution maps in Figs. 3(b) and (c) illustrate that due to solute redistribution during

solidification, Nb is accumulated in β dendrites, whereas Ti is rejected into the liquid resulting in higher concentration of Ti in interdendritic zones. This segregation pattern is a consequence of higher melting point of Nb which causes this element to have a partition coefficient higher than one when it dissolves in Ti. In contrast, Fig. 3(d) indicates that Fe presents a more uniform distribution across the whole area which is due to its high diffusion rate in Ti [34]. Similar results were obtained in a Ti-Nb-Sn alloy system [35] where Nb, with a higher melting point and partition coefficient greater than unit level, is segregated in the dendritic areas whereas Sn, with lower melting point and a partition coefficient less than one, and Ti are concentrated in interdendritic areas.

Studies show that the presence of more β-stabiliser (e.g. Nb) in dendrites and its lower concentration in interdendritic regions can cause martensite transformation e.g. β→α", mainly in interdendritic zones [36, 37]. In our work, the α" martensite formation is not completely suppressed in Ti-7Fe-9Nb alloy (Fig. 1 and Fig. 2) and it is expected that this minor martensitic transformation occurs mainly in the interdendritic zones which contain less Nb. The presence of α" can affect the mechanical properties of Ti alloys which will be discussed in the next section. In the case of Ti-7Fe-11Nb alloy with the highest Nb content and Mo_{eq} value, and despite its dendritic microstructure, the martensitic transformation is suppressed, suggesting that the Nb concentration in the interdendritic regions may still be high enough to stabilise β phase during quenching of the alloy.

3.2. Mechanical properties

The mechanical properties of the titanium alloys are largely affected by the constituent phases and their volume fraction [38]. As such, to investigate the influence of composition on the mechanical behavior of the alloys, compressive mechanical testing and Vickers hardness measurements were carried out. Generally, a compressive test is not as sensitive as a tensile test to minor processing flaws which lead to premature failure. Consequently, compressive testing results can display the

intrinsic behaviour (strength/work hardening) of the material and can be used to predict its tensile properties [39, 40].

Fig. 4 displays the typical compressive stress-strain curves of the series of Ti-7Fe-xNb alloys at room temperature. The compressive test was stopped either after failure of the alloy or when the maximum load capacity (100 kN) of the test machine was reached. According to Fig. 4, Nb addition impacts strongly the mechanical properties of the alloys. With the exception of Ti-7Fe and Ti-7Fe-1Nb, the alloys did not fail during compressive testing even after being largely deformed by ~42% in the case of Ti-7Fe-11Nb alloy. From Fig. 4, the 0.2% proof compressive yield stress and the plastic strain of the alloys were measured and their variations, with respect to the concentration of Nb (wt% Nb) are presented in Fig. 5. It can be inferred from Fig. 5 that the compressive yield strength of all alloys are higher than those of CP-Ti (552 MPa) [41] and Ti-6Al-4V (970 MPa) [42] alloys. Additionally, both compressive yield strength and plastic strain of the alloys are influenced by Nb content. As can be seen, Ti-7Fe, the least stable alloy (Mo_{eq} = 17.5 wt%) that does not contain Nb, exhibits the highest yield strength (1847 MPa) and the lowest plastic strain (2%). This can be attributed to the existence of the highest concentration of α" martensite phase in its microstructure which is evident from Table 1 and Fig. 2(a). Since the orthorhombic crystal structure of α" phase contains less slip systems than the bcc crystal structure of β phase, higher stress is needed for plastic deformation of α" phase than for the β phase matrix [43].

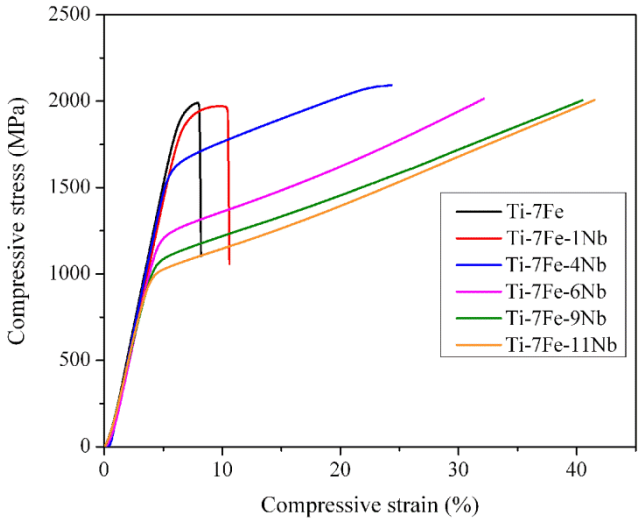

Fig. 4 Compressive stress–strain curves of Ti–7Fe–xNb alloys at room temperature.

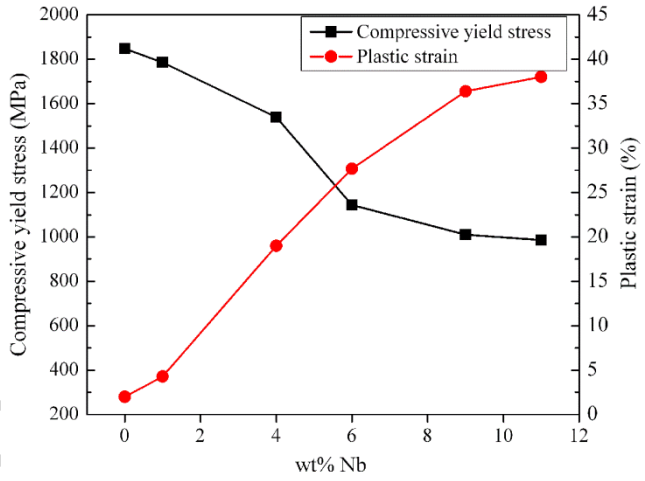

Fig. 5 Compressive yield stress and plastic strain of Ti-7Fe-xNb alloys.

Conversely, according to Fig. 5, the yield strength of the alloys is reduced and their plastic strain is improved substantially with increasing Nb concentration. It is widely known that Nb is a β stabilizer element [11]. As more Nb is added to the alloys, the Mo_{eq} is enhanced which implies an increase in β phase stability and a reduction in the concentration of high strength brittle α" phase of the alloys, as can also be inferred from Table 1. Consequently, in the present study, Ti-7Fe-11Nb alloy with the highest Nb content and dominant β phase microstructure possesses the lowest yield strength which is still greater than those of the best commercial Ti-based biomaterials, e.g. CP-Ti and Ti-6Al-4V as mentioned above. The higher yield strength enhances the capacity of the

alloy against its permanent shape change which could benefit the patient [44]. Moreover, due to the high plasticity of β phase structure [11], this alloy also presents the highest plastic strain (38%) among the alloys when the maximum load capacity (100 kN) of the test machine was reached and the test was stopped. The high plastic strain of this alloy indicates its good workability at room temperature.

The elastic modulus values of the alloys are shown in Fig. 6. As seen in Fig. 6, the Young's modulus values of the alloys decrease with the increase in their Nb content. Among all alloys, Ti-7Fe, which has the least stable β phase microstructure (Mo_{eq} = 17.5 wt%) and contains the greatest proportion of α" phase, presents the highest Young's modulus (129 GPa). When 1 or 4 wt% Nb is added to this alloy, the Young's modulus reduces subsequently. Further increases in Nb content (6, 9, 11 wt %) and hence β phase stability, lead to more reductions in the values of Young's modulus of the alloys as displayed in Fig. 6. These results may be associated with the formation possibility of martensitic α" phase during quenching [38]. In this work, α" phase is found in all alloys except Ti-7Fe-11Nb, especially in Ti-7Fe, Ti-7Fe-1Nb and Ti-7Fe-4Nb alloys with low Nb contents. As explained earlier, with an increase in β-stabilizer Nb content, the likelihood of the alloys undergoing a β→α" martensitic transformation, hence the volume fraction of α" martensite in their microstructure is reduced. This results in a progressive decline in Young's modulus values of the alloys reaching the minimum (84 GPa) in Ti-7Fe-11Nb alloy which has the highest concentration of Nb and a single β phase microstructure (Mo_{eq} = 20.56 wt%). In the present study, among the alloys, the Young's modulus values of Ti-7Fe-6Nb, Ti-7Fe-9Nb and Ti-7Fe-11Nb are smaller than those of commercially used biomedical Ti alloys, e.g. CP-Ti (104 GPa) [19] and Ti–6Al–4V (114 GPa) [45]. The achieved results for Young's modulus agree with those for various phases of Ti alloys, where the Young's modulus of the phases increases in the sequence of β < α" < α' < ω [23, 46].

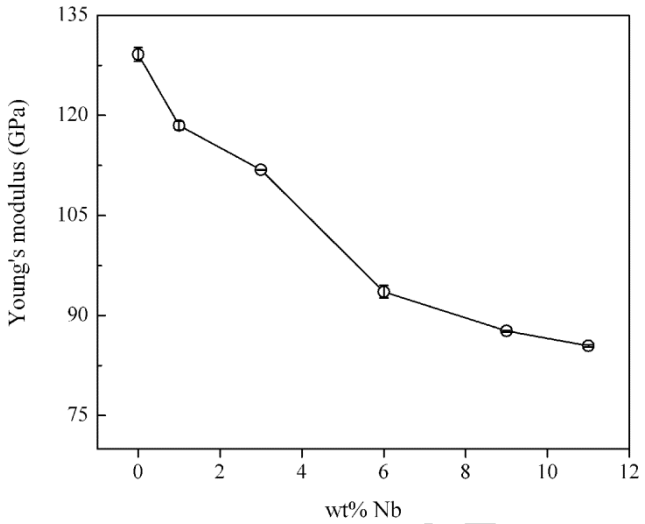

Fig. 6 Young's modulus of Ti-7Fe-xNb alloys.

Fig. 7 shows the SEM micrographs of the fracture surfaces for the Ti-7Fe and Ti-7Fe-1Nb alloys after a compressive test. Since the Ti-7Fe-xNb (x= 4, 6, 9, 11) series alloys did not fail during a compressive test, their fractographies were not examined. As shown in Fig. 7(a), Ti-7Fe is characterised by cleavage facets together with some dimpled surfaces which are shallow, smooth and small in size. This feature corresponds to the less ductile nature of the specimen as is also indicated by the low value of compressive strain (8%). As can be seen in Fig. 7(b), the fracture surface of Ti-7Fe-1Nb alloy contains more dimples which are larger and rougher in some areas. This is related to the increase in the ductility of this alloy with addition of 1 wt% Nb, which is consistent with the compressive strain of 11%.

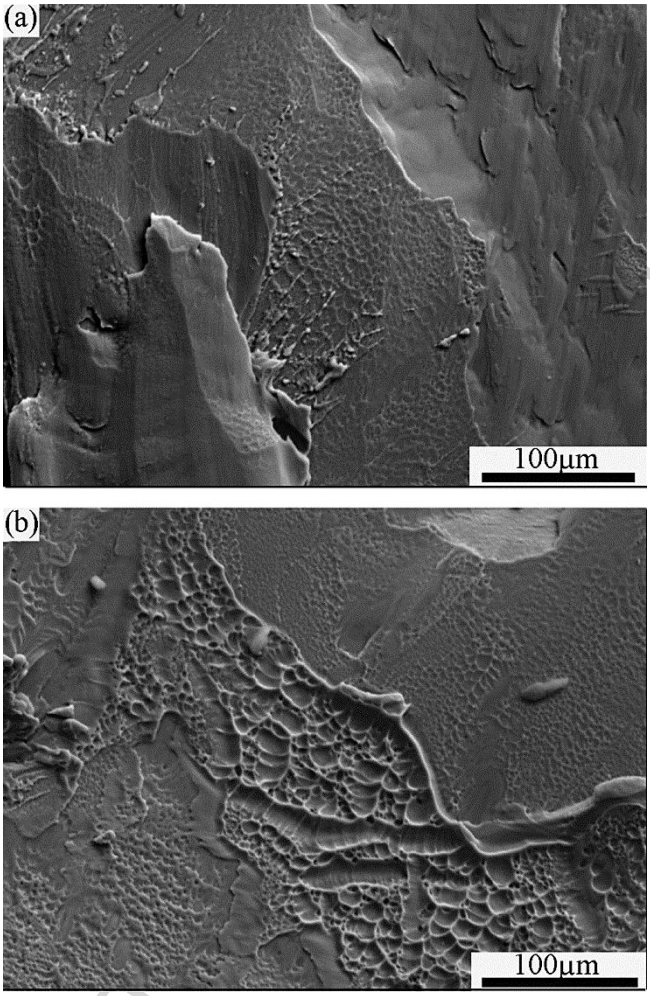

Fig. 7 SEM fractographic morphologies of (a) Ti-7Fe and (b) Ti-7Fe-1Nb alloys after compressive testing.

Fig. 8 displays the Vickers hardness values of the studied alloys. The results show that the Vickers hardness of all alloys are higher than those of commercially used biomedical Ti alloys, e.g. CP-Ti (190 Hv) [22] and Ti–6Al–4V (294 Hv) [47]. Additionally, the Vickers hardness values of the alloys are influenced by Nb content. The highest Vickers hardness is found for Ti-7Fe (560 Hv) which contains the highest concentration of α" phase (V_f = 38%). With further addition of β-stabilizer Nb, up to 11 wt%, hence an increase in β-phase stability, the hardness of the alloys declines reaching the minimum in single β Ti-7Fe-11Nb (325 Hv). Yet, it is still greater than those of commercially used CP-Ti and Ti–6Al–4V as mentioned above. The α" martensitic phase has greater hardness than β phase [46]. As such, the observed decrease in the measured Vickers hardness values of Ti-7Fe-xNb alloys with addition of Nb, can be attributed to the decrease in their α" phase concentration which is evident from Table 1 and Fig. 2. The measured Vickers

hardness values are very similar to those for other titanium alloys containing Nb. For example, the Vickers hardness values are between 289 and 479 Hv for Ti–xNb–3Fe alloys (x = 10, 15, 20, 25 wt%) [48], between 400 and 500 Hv for Ti–Nb–Zr–X (X = Cr, Fe, Ta) alloys [49] and in the range of 412-575 Hv for the Ti–Cr–xNb (x = 10, 20, 30 at%) alloy system [50].

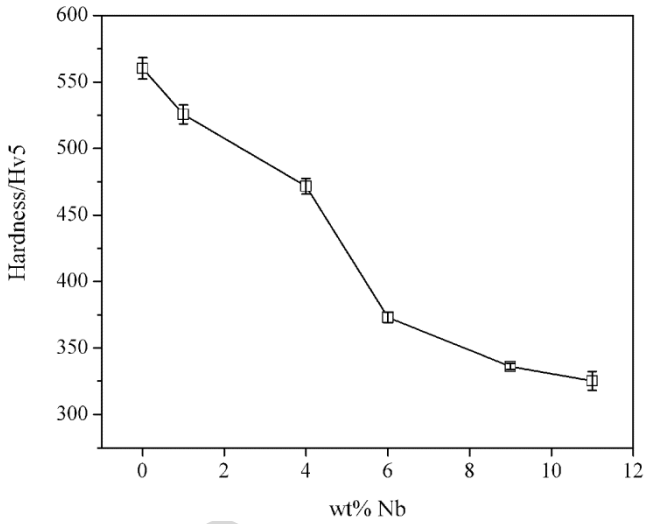

Fig. 8 Vickers hardness of Ti–7Fe–xNb alloys.

Researchers have demonstrated an association between the wear characteristics and hardness of the materials which suggests that wear resistance improves with increasing hardness [51, 52]. As such, according to the Vickers hardness values, it is expected that all designed alloys will have better wear resistance than CP-Ti and Ti-6Al-4V alloys. This can result in the reduction of wear debris which may prevent loosening of implants and increase their longevity in the human body [53].

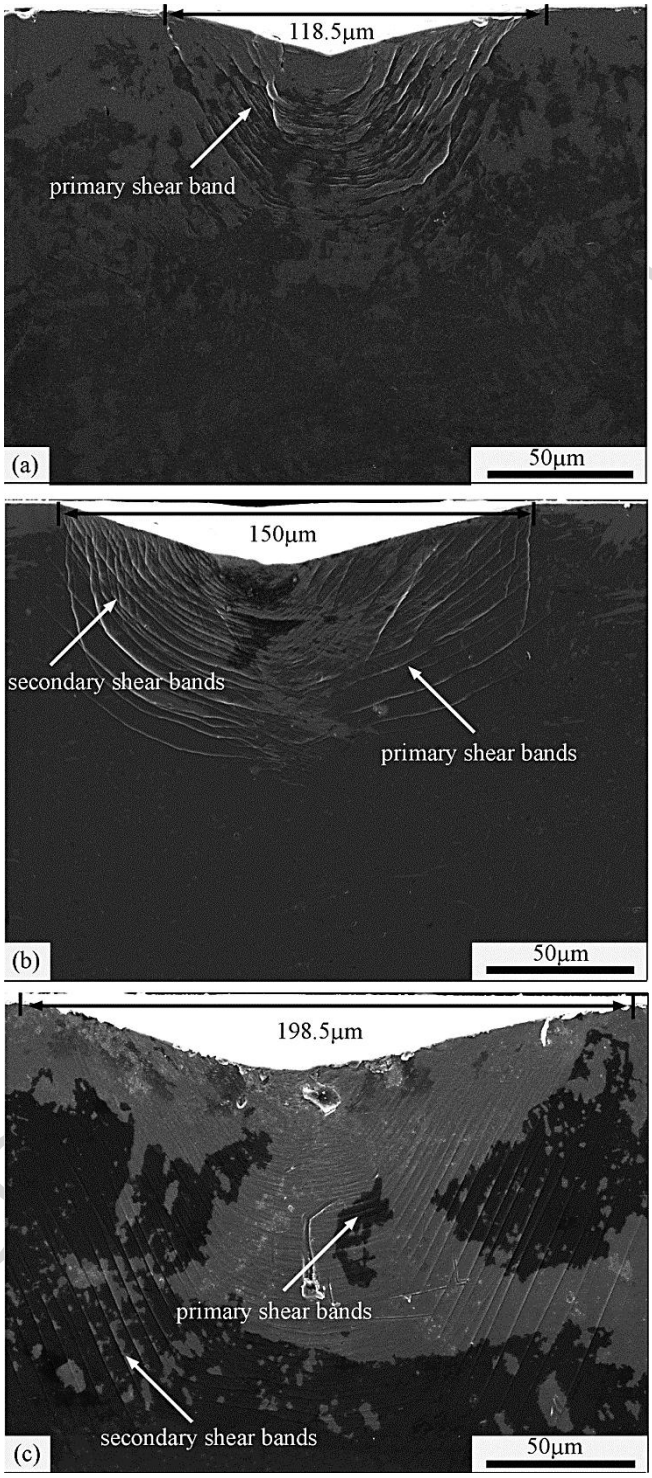

Fig. 9 The morphologies of the plastic deformation zones beneath Vickers indenter in: (a) Ti–7Fe, (b) Ti–7Fe–4Nb, and (c) Ti–7Fe–11Nb alloys.

Fig. 9 illustrates the deformation region underneath the Vickers indenter in Ti-7Fe, Ti-7Fe-4Nb and Ti-7Fe-11Nb alloys. Notably, with the increase in Nb content of the alloys, hence decrease in their Vickers hardness values, the penetration of the indenter in the alloys' surface and the lateral

size of the indentation both increase. Additionally, in all three alloys, immediately surrounding the bulge area (tip of the indent), several semi-circular slip-steps called primary shear bands [21] can be seen. Interestingly, in Ti-7Fe-4Nb and Ti-7Fe-11Nb alloys (Figs. 9(b) and (c)) with higher Nb content, additional radial slip-steps named secondary shear bands, initiating along the indentation surface in a form of straight lines [21], can be observed.

It is clear that the density of primary shear bands is greater than that of the secondary ones. The shear bands are produced when the local stress exceeds the yield point [21] and materials deform plastically. They are formed as a consequence of the highly localized deformation during indentation. To be more precise, the presence of shear bands indicates excessive deformation as a result of strain localization [38, 54]. It has been reported that during indentation, the primary shear bands are activated first from the stress produced by the applied load and then, to accommodate further plastic deformation, the secondary shear bands emanate [20].

Generally, for materials with good plastic deformation ability, when the indenter penetrates their surface, the subsurface materials near the indenter tip are deformed due to hydrostatic pressure and are hardened subsequently by the applied plastic deformation. Under such conditions, the stress is not enough to produce further plastic deformation in this region. However, this hardened area could compress the near materials and cause this area to deform plastically which results in the formation of shear bands. Likewise, once this part also becomes hardened, it could produce plastic deformation in the adjacent materials, therefore shear bands formation could extend to adjacent areas beneath the indented surface [55]. In this work, Ti-7Fe-11Nb alloy presents a larger deformation zone, with more primary and secondary shear bands beneath indent, than Ti-7Fe and Ti-7Fe-4Nb alloys (Fig. 9(c)). This is due to its microstructure which consists of β phase with higher plastic deformation ability than α" phase [56]. Notably, in the Ti-7Fe-4Nb alloy with a lower β-stabiliser Nb content, the size of the plastic deformation zone and the number of primary and secondary shear bands observed are reduced (Fig. 9(b)). This can be attributed to its higher concentration of α" martensitic phase and an associated lower plastic deformation ability than β phase [56] that causes plastic deformation to be concentrated only in a smaller region

beneath the indenter tip. Finally, in case of Ti-7Fe alloy, with highest volume fraction of α" phase, the size of the deformation zone and the amount of the observed primary shear bands are minimised while no secondary ones can be seen in Fig. 9(a).

Based on these experimental results, it is suggested that addition of Nb can considerably reduce the formation of α" martensite and enhance the stability of β phase, hence improving the mechanical properties of Ti-Fe based alloy required for biomedical application. However, it would be interesting to compare Nb with other alloying elements (e.g. Mo, Zr, Ta) for their effects on the phase stability and the mechanical properties of the Ti-Fe alloy and then select the best alloying element for future studies.

4. Conclusion

This work investigated the effects of Nb on the β phase stability and the resulting microstructure and mechanical properties of the designed Ti-Fe-Nb alloys. The results revealed that Ti-7Fe-xNb alloys can include β and α" phases, the proportions of which depend on the amount of β-stabilizer Nb. As more Nb (1, 4, 6, 9 wt%) is introduced into the Ti-7Fe alloy, the proportion of α" phase declines until at 11 wt% no α" phase remains. Instead, the alloy microstructure only includes β phase with a bcc crystal structure. It is proposed that increasing the Nb content enhances the β phase stability of the designed alloys against β→α" martensitic transformation during rapid cooling.

The hardness (325-520 Hv) and compressive yield strength (985-1847 MPa) of Ti-7Fe and Ti-7Fe-xNb alloys varied depending on the relative proportions of β and α" phases. However, they were better than for the best commercial Ti-based biomaterials, CP-Ti (190 Hv, 552 MPa) and Ti-6Al-4V (294 Hv, 970 MPa) alloys. Progressively increasing the Nb content from 0 to 11 wt%, reduced the Young's modulus values from 129 GPa to 84 GPa, thus providing a much lower elastic modulus than for CP-Ti (104 GPa) and Ti–6Al–4V (114 GPa). Moreover, Ti-7Fe-11Nb alloy exhibited the highest plastic deformation, indicating its good workability at room temperature. It also presented the highest numbers of primary and secondary shear bands beneath

the Vickers indenter due to its dominant β phase microstructure.

Reference

[1] H.-C. Hsu, S.-K. Hsu, S.-C. Wu, C.-J. Lee, W.-F. Ho, Structure and mechanical properties of as-cast Ti–5Nb–xFe alloys, Mater. Charact. 61 (2010) 851-858.

[2] B. Song, S. Dong, B. Zhang, H. Liao, C. Coddet, Effects of processing parameters on microstructure and mechanical property of selective laser melted Ti6Al4V, Mater. Des. 35 (2012) 120-125.

[3] M. Niinomi, M. Nakai, J. Hieda, Development of new metallic alloys for biomedical applications, Acta Biomater. 8 (2012) 3888-3903.

[4] H. Attar, M. Calin, L.C. Zhang, S. Scudino, J. Eckert, Manufacture by selective laser melting and mechanical behavior of commercially pure titanium, Mater. Sci. Eng. A 593 (2014) 170-177.

[5] W.-F. Ho, S.-C. Wu, S.-K. Hsu, Y.-C. Li, H.-C. Hsu, Effects of molybdenum content on the structure and mechanical properties of as-cast Ti–10Zr-based alloys for biomedical applications, Mater. Sci. Eng. C 32 (2012) 517-522.

[6] W.-F. Ho, C.-H. Pan, S.-C. Wu, H.-C. Hsu, Mechanical properties and deformation behavior of Ti–5Cr–xFe alloys, J. Alloys Compd. 472 (2009) 546-550.

[7] D. Kuroda, M. Niinomi, M. Morinaga, Y. Kato, T. Yashiro, Design and mechanical properties of new β type titanium alloys for implant materials, Mater. Sci. Eng. A 243 (1998) 244-249.

[8] M. Abdel-Hady Gepreel, M. Niinomi, Biocompatibility of Ti-alloys for long-term implantation, J. Mech. Behav. Biomed. Mater. 20 (2013) 407-415.

[9] Y.L. Hao, Z.B. Zhang, S.J. Li, R. Yang, Microstructure and mechanical behavior of a Ti–24Nb–4Zr–8Sn alloy processed by warm swaging and warm rolling, Acta Mater. 60 (2012) 2169-2177.

[10] I. Milošev, G. Žerjav, J.M. Calderon Moreno, M. Popa, Electrochemical properties,

chemical composition and thickness of passive film formed on novel Ti–20Nb–10Zr–5Ta alloy, Electrochim. Acta 99 (2013) 176-189.

[11] G. He, J. Eckert, Q.L. Dai, M.L. Sui, W. Löser, M. Hagiwara, E. Ma, Nanostructured Ti-based multi-component alloys with potential for biomedical applications, Biomaterials 24 (2003) 5115-5120.

[12] L.C. Zhang, D. Klemm, J. Eckert, Y.L. Hao, T.B. Sercombe, Manufacture by selective laser melting and mechanical behavior of a biomedical Ti–24Nb–4Zr–8Sn alloy, Scr. Mater. 65 (2011) 21-24.

[13] D. Kent, G. Wang, M. Dargusch, Effects of phase stability and processing on the mechanical properties of Ti–Nb based β Ti alloys, J. Mech. Behav. Biomed. Mater. 28 (2013) 15-25.

[14] D. Kuroda, H. Kawasaki, A. Yamamoto, S. Hiromoto, T. Hanawa, Mechanical properties and microstructures of new Ti–Fe–Ta and Ti–Fe–Ta–Zr system alloys, Mater. Sci. Eng. C 25 (2005) 312-320.

[15] W. Xu, K.B. Kim, J. Das, M. Calin, J. Eckert, Phase stability and its effect on the deformation behavior of Ti–Nb–Ta–In/Cr β alloys, Scripta Mater. 54 (2006) 1943-1948.

[16] S.E. Haghighi, K. Janghorban, S. Izadi, Structural evolution of Fe–50at.% Al powders during mechanical alloying and subsequent annealing processes, 495 (2010) 260-264.

[17] L.C. Zhang, Z. Shen, J. Xu, Glass formation in a (Ti, Zr, Hf)–(Cu, Ni, Ag)–Al high-order alloy system by mechanical alloying, J. Mater. Res. 18 (2003) 2141-2149.

[18] H. Yang, J. Wen, M. Quan, J. Wang, Evaluation of the volume fraction of nanocrystals devitrified in Al-based amorphous alloys, J. Non-Cryst. Solids 355 (2009) 235-238.

[19] S. Ozan, J. Lin, Y. Li, R. Ipek, C. Wen, Development of Ti–Nb–Zr alloys with high elastic admissible strain for temporary orthopedic devices, Acta Biomater. 20 (2015) 176-187.

[20] H. Xie, Y. Li, S. Liao, P. Hodgson, C.e. Wen, Plastic deformation in a partially crystallized Zr-based BMG under Vickers indenter, J. Alloys Compd. 484 (2009) 886-890.

[21] H. Xie, Y. Li, D. Yang, P. Hodgson, C.e. Wen, Plastic deformation in the annealed Zr_{41}–

Ti_{14}–$Cu_{12.5}$–Ni_{10}–$Be_{22.5}$ bulk metal glass under indenter, J. Alloys Compd. 475 (2009) 501-505.

[22] D.J. Lin, J.H. Chern Lin, C.P. Ju, Structure and properties of Ti–7.5Mo–xFe alloys, Biomaterials 23 (2002) 1723-1730.

[23] Y.L. Zhou, M. Niinomi, T. Akahori, Effects of Ta content on Young's modulus and tensile properties of binary Ti–Ta alloys for biomedical applications, Mater. Sci. Eng. A 371 (2004) 283-290.

[24] E.W. Collings. Nonequilibrium phases. The physical metallurgy of titanium allloys. American society for metals, USA, 1984. pp. 75-110.

[25] M. Morinaga, N. Yukawa, T. Maya, K. Sone, H. Adachi. Theoretical design of titanium alloys. Sixth World Conference on Titanium. III, 1988. p.1601-1606.

[26] X.H. Min, S. Emura, N. Sekido, T. Nishimura, K. Tsuchiya, K. Tsuzaki, Effects of Fe addition on tensile deformation mode and crevice corrosion resistance in Ti–15Mo alloy, Mater. Sci. Eng. A 527 (2010) 2693-2701.

[27] M. Ahmed, D. Wexler, G. Casillas, O.M. Ivasishin, E.V. Pereloma, The influence of β phase stability on deformation mode and compressive mechanical properties of Ti–10V–3Fe–3Al alloy, Acta Mater. 84 (2015) 124-135.

[28] G. Welsch, R. Boyer, E. Collings. Materials properties handbook: titanium alloys. Forth ed., ASM international, Ohio, 1993.

[29] S.B. Gabriel, J.V.P. Panaino, I.D. Santos, L.S. Araujo, P.R. Mei, L.H. de Almeida, C.A. Nunes, Characterization of a new beta titanium alloy, Ti–12Mo–3Nb, for biomedical applications, J. Alloys Compd. 536, Supplement 1 (2012) S208-S210.

[30] E.S.N. Lopes, A. Cremasco, C.R.M. Afonso, R. Caram, Effects of double aging heat treatment on the microstructure, Vickers hardness and elastic modulus of Ti–Nb alloys, Mater. Charact. 62 (2011) 673-680.

[31] S.B. Gabriel, J. Dille, C.A. Nunes, G.d.A. Soares, The effect of niobium content on the hardness and elastic modulus of heat-treated Ti-10Mo-xNb alloys, Mater. Res. 13 (2010) 333-337.

[32] Y. Mantani, M. Tajima, Phase transformation of quenched α″ martensite by aging in Ti–

Nb alloys, Mater. Sci. Eng. A 438–440 (2006) 315-319.

[33] C.Y. Cui, D.H. Ping, Microstructural evolution and ductility improvement of a Ti–30Nb alloy with Pd addition, J. Alloys Compd. 471 (2009) 248-252.

[34] B. Liu, Y. Li, H. Matsumoto, Y. Liu, Y. Liu, A. Chiba, Thermomechanical characterization of P/M Ti–Fe–Mo–Y alloy with a fine lamellar microstructure, Mater. Sci. Eng. A 528 (2011) 2345-2352.

[35] P.E. Moraes, R.J. Contieri, E.S. Lopes, A. Robin, R. Caram, Effects of Sn addition on the microstructure, mechanical properties and corrosion behavior of Ti–Nb–Sn alloys, Mater. Charact. 96 (2014) 273-281.

[36] J.P. Liu, Y.D. Wang, Y.L. Hao, H.L. Wang, Y. Wang, Z.H. Nie, R. Su, D. Wang, Y. Ren, Z.P. Lu, J.G. Wang, X.D. Hui, R. Yang, High-energy X-ray diffuse scattering studies on deformation-induced spatially confined martensitic transformations in multifunctional Ti–24Nb–4Zr–8Sn alloy, Acta Mater. 81 (2014) 476-486.

[37] D.Q. Martins, M.E.P. Souza, S.A. Souza, D.C. Andrade, C.M.A. Freire, R. Caram, Solute segregation and its influence on the microstructure and electrochemical behavior of Ti–Nb–Zr alloys, J. Alloys Compd. 478 (2009) 111-116.

[38] S. Ehtemam Haghighi, H.B. Lu, G.Y. Jian, G.H. Cao, D. Habibi, L.C. Zhang, Effect of α″ martensite on the microstructure and mechanical properties of beta-type Ti–Fe–Ta alloys, Mater. Des. 76 (2015) 47-54.

[39] H. Attar, M. Bönisch, M. Calin, L.-C. Zhang, S. Scudino, J. Eckert, Selective laser melting of in situ titanium–titanium boride composites: Processing, microstructure and mechanical properties, Acta Mater. 76 (2014) 13-22.

[40] L.C. Zhang, J. Das, H.B. Lu, C. Duhamel, M. Calin, J. Eckert, High strength Ti–Fe–Sn ultrafine composites with large plasticity, Scripta Mater. 57 (2007) 101-104.

[41] G. Welsch, R. Boyer, E.W. Collings. Materials Properties Handbook: Titanium alloys, ASM International, 1994.

[42] W. Yan, J. Berthe, C. Wen, Numerical investigation of the effect of porous titanium

femoral prosthesis on bone remodeling, Mater. Des. 32 (2011) 1776-1782.

[43] Y. Ren, F. Wang, S. Wang, C. Tan, X. Yu, J. Jiang, H. Cai, Mechanical response and effects of β-to-α" phase transformation on the strengthening of Ti–10V–2Fe–3Al during one-dimensional shock loading, Mater. Sci. Eng. A 562 (2013) 137-143.

[44] M. Calin, A. Gebert, A.C. Ghinea, P.F. Gostin, S. Abdi, C. Mickel, J. Eckert, Designing biocompatible Ti-based metallic glasses for implant applications, Mater. Sci. Eng. C 33 (2013) 875-883.

[45] L. Bolzoni, E.M. Ruiz-Navas, E. Gordo, Feasibility study of the production of biomedical Ti–6Al–4V alloy by powder metallurgy, Mater. Sci. Eng. C 49 (2015) 400-407.

[46] Y. Zhu, X. Wang, L. Wang, Y. Fu, J. Qin, W. Lu, D. Zhang, Influence of forging deformation and heat treatment on microstructure of Ti–xNb–3Zr–2Ta alloys, Mater. Sci. Eng. C 32 (2012) 126-132.

[47] Y.-Y. Chen, L.-J. Xu, Z.-G. Liu, F.-T. Kong, Z.-Y. Chen, Microstructures and properties of titanium alloys Ti-Mo for dental use, Trans. Nonferrous Met. Soc. China 16, Supplement 2 (2006) s824-s828.

[48] J.M. Chaves, O. Florêncio, P.S. Silva Jr, P.W.B. Marques, C.R.M. Afonso, Influence of phase transformations on dynamical elastic modulus and anelasticity of beta Ti–Nb–Fe alloys for biomedical applications, J. Mech. Behav. Biomed. Mater. 46 (2015) 184-196.

[49] M. Niinomi, T. Akahori, T. Takeuchi, S. Katsura, H. Fukui, H. Toda, Mechanical properties and cyto-toxicity of new beta type titanium alloy with low melting points for dental applications, Mater. Sci. Eng. C 25 (2005) 417-425.

[50] L. Slokar, T. Matković, P. Matković, Alloy design and property evaluation of new Ti–Cr–Nb alloys, Mater. Des. 33 (2012) 26-30.

[51] L.-J. Xu, S.-L. Xiao, J. Tian, Y.-Y. Chen, Microstructure, mechanical properties and dry wear resistance of β-type Ti–15Mo–xNb alloys for biomedical applications, Trans. Nonferrous Met. Soc. China 23 (2013) 692-698.

[52] D.I. Adebiyi, A.P.I. Popoola, Mitigation of abrasive wear damage of Ti–6Al–4V by laser

surface alloying, Mater. Des. 74 (2015) 67-75.

[53] M. Geetha, A.K. Singh, R. Asokamani, A.K. Gogia, Ti based biomaterials, the ultimate choice for orthopaedic implants – A review, Prog. Mater Sci. 54 (2009) 397-425.

[54] P. Manda, U. Chakkingal, A.K. Singh, Hardness characteristic and shear band formation in metastable β-titanium alloys, Mater. Charact. 96 (2014) 151-157.

[55] P. Zhang, S.X. Li, Z.F. Zhang, General relationship between strength and hardness, Mater. Sci. Eng. A 529 (2011) 62-73.

[56] L. Qu, Z.N. Yang, F.C. Zhang, M. Zhang, X.Y. Zhang, R.P. Liu, Effect of deformation and heat treatment on the microstructure and mechanical properties of β-Zr40Ti5Al4V alloy, J. Alloys Compd. 612 (2014) 80-89.

Figure captions:

Fig. 1 XRD patterns of the as-cast Ti–7Fe–xNb alloys.

Fig. 2 Optical micrographs of Ti–7Fe–xNb alloys: (a) Ti–7Fe, (b) Ti–7Fe–1Nb, (c) Ti–7Fe–4Nb, (d) Ti–7Fe–6Nb, (e) Ti–7Fe–9Nb, and (f) Ti–7Fe–11Nb.

Fig. 3 (a) Backscattered SEM image of Ti–7Fe–11Nb alloy and its X–ray element distribution maps: (b) Nb distribution, (c) Ti distribution and (d) Fe distribution.

Fig. 4 Compressive stress–strain curves of Ti–7Fe–xNb alloys at room temperature.

Fig. 5 Compressive yield stress and plastic strain of Ti-7Fe-xNb alloys.

Fig. 6 Young's modulus of Ti–7Fe–xNb alloys.

Fig. 7 SEM fractographic morphologies of: (a) Ti-7Fe and (b) Ti-7Fe-1Nb alloys after compressive testing.

Fig. 8 Vickers hardness of Ti–7Fe–xNb alloys.

Fig. 9 The morphologies of the plastic deformation zones beneath Vickers indenter in: (a) Ti–7Fe, (b) Ti–7Fe–4Nb, and (c) Ti–7Fe–11Nb alloys.

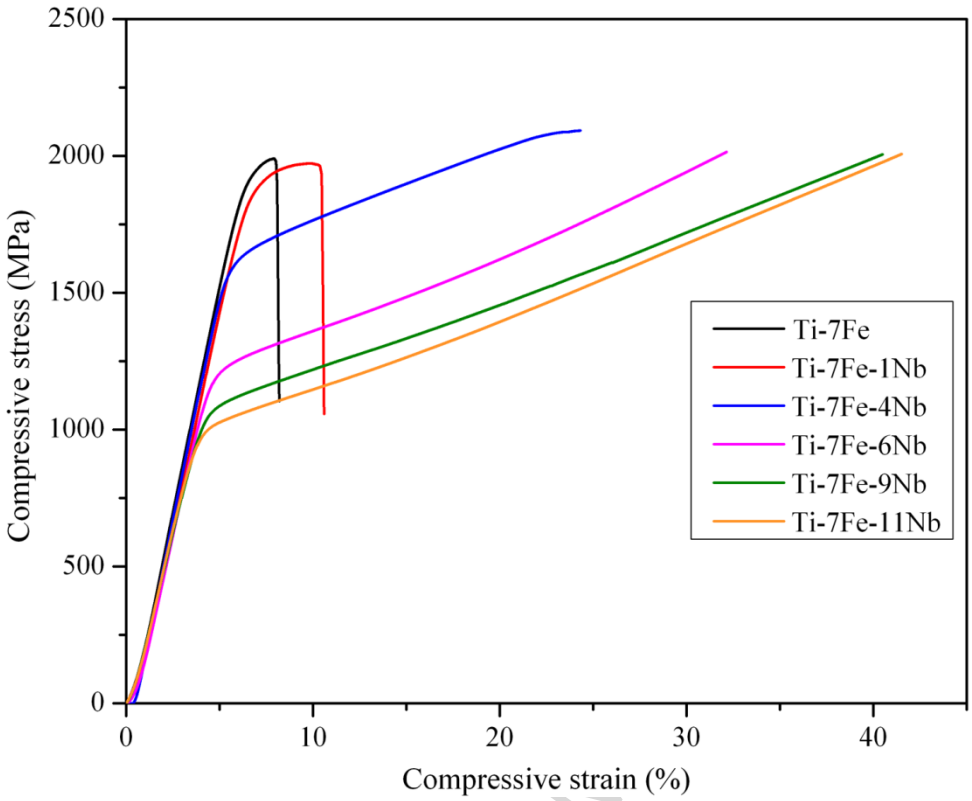

Graphical abstract

Highlight

- Nb addition affects the β phase stability and α″ martensitic phase transformation.
- Adding 11 wt% Nb is enough to retain only β phase.
- All alloys exhibit hardness and strength higher than those of Ti-6Al-4V and CP-Ti.
- Ti-7Fe-11Nb alloy presents the lowest elastic modulus and largest plastic strain.